Chapter 15
Basins of attraction in a simple harvesting system with a stopper

Marek Borowiec, Grzegorz Litak, Stefano Lenci

Abstract We examine the dynamical response and the power output of a vibration energy harvesting electro-mechanical system with kinematic ambient excitation and impact. Due to the stopper non-linearities the examined system exhibits multiple solutions. We characterize their properties and stability by the voltage output and corresponding basins of attraction.

15.1 Introduction

Many mechanical systems, with non-linearities show complex responses characterized by multiple solutions with different amplitudes of vibrations and specific basins of attraction. Their existence make unrivalled opportunity to improve the effectiveness of kinetic energy harvester through so called broadband frequency effect [1, 2, 3, 4]. Corresponding energy harvesting devices are equipment by mechanical resonators and appropriate energy transducers, transforming ambient mechanical energy into electric form.

Recently, the concept kinetic energy harvester model based on mechanical resonator and electromagnetic transducers [5, 6, 7] was explored extensively. This work were continued by Blystad and Halvorsen [8]. The electrostatic devices of micro-electromechanical systems (MEMS) were proposed and studied by Gu [9] and Le et al. [10, 11].

G. Litak and M. Borowiec
Faculty of Mechanical Engineering, Lublin University of Technology, Nadbystrzycka 36, PL-20-618 Lublin, Poland
S. Lenci
Department of Civil and Building Engineering, and Architecture, Polytechnic University of Marche, 60131 Ancona, Italy
G. Litak e-mail: g.litak@pollub.pl, M. Borowiec e-mail: g.litak@pollub.pl, S. Lenci e-mail: lenci@univpm.it

In the present chapter we continue study on the non-linear impacting electro-magnetic harvesters with stoppers, derived from the idea of Soliman et al. [12, 13]. For the present system, at least two different solutions appear due to applied a stopper of the moving structure, if the amplitude of mechanical resonator is large enough. The impacting to the stopper both limits vertical displacements and simultaneously changes the elastic characteristics of the system.

15.2 The model

The model of energy harvester is made up of a main body frame, which consists both the electrical harvester and the internal mechanical system (see Fig. 15.1a). The subsystem within the frame includes the effective magnet mass m which adopts the frame vibrations through the springs and dampers. The frame system is vertically moving due to a ground harmonic excitation $y = A\cos(\omega_e t)$. The mounted transducer on the frame, harvests the kinetic energy, converting into electric one. This energy transformation causes the electric damper b_e via relative velocity of the vibrating effective mass as a magnet, and the coil located appropriately on the frame.

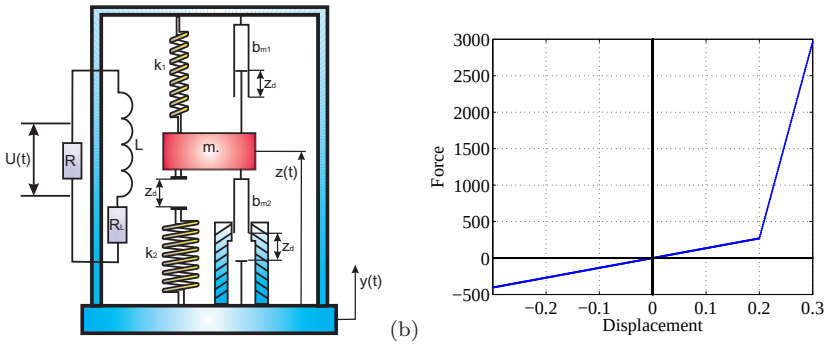

Fig. 15.1 Schematics of the mechanical resonator of energy harvesting system (a). The additional electrical circuit is powered by Faraday electromotive force via the moving coil across the magnetic field. In the calculations we neglect self-induction of the coil L_c. The stiffness characteristics of the effective model (b).

When a distance z_d is covered by mass m and hits onto a spring k_2 occurs, the spring stiffness k is changing as shown in Fig. 15.1b. Due to impacts both the stiffness k and the mechanical damping b_m take two differently values ($i = 1$ and $i = 2$), from k_1 and b_{m1} when impacts does not take place,

to k_2 and b_{m2}, while contacting. And then the mechanical restoring force F_r is simultaneously modifying according to the Eq. 15.1:

$$F_r = \begin{cases} k_1 z & \text{for} \quad z < z_d \ (i = 1) \\ k_2 z + (k_1 - k_2) z_d & \text{for} \quad z \geq z_d \ (i = 2) \end{cases} \tag{15.1}$$

as well the damping restoring force F_d:

$$F_d = \begin{cases} b_1 \dot{z}, & \text{for} \quad z < z_d \ (i = 1) \\ b_2 \dot{z}, & \text{for} \quad z \geq z_d \ (i = 2) \end{cases} \tag{15.2}$$

Equation of motion of the system reads

$$m\ddot{z} + b_i \dot{z} + k_i z = -m\ddot{y} + (k_2 - k_1) z_d \Theta(z - z_d). \tag{15.3}$$

Finally, voltage induced across the load resistor R can be estimated as

$$U = \frac{RB\ell}{R + R_c} \dot{z}. \tag{15.4}$$

where R, R_c denote corresponding the load and the coils resistances, B is the magnetic induction and ℓ is the coil effective length.

Using the dimensionless variables:

$$\tau = \omega_1 t, \quad \Omega = \frac{\omega_e}{\omega_1}, \quad \mathcal{Z} = \frac{z}{z_d}, \quad \mathcal{Y} = \frac{y}{z_d}, \tag{15.5}$$

where the natural frequency used for introducing dimensionless time τ is $\omega_1 = \sqrt{k_1/m}$.

The equation of motion in dimensionless form becomes:

$$\ddot{\mathcal{Z}} + 2\eta_i \dot{\mathcal{Z}} + r_i^2 \mathcal{Z} = -\ddot{\mathcal{Y}} + (\rho^2 - 1)\Theta(\mathcal{Z} - 1) \tag{15.6}$$

The function $\Theta(\mathcal{Z}-1)$ is the Heaviside function, switching the system whether the mass m is in contact with the spring of stiffness k_2 or not.

The parameters r and η depend on conditions of Eqs. 15.1, 15.2 and for two cases ($i = 1, 2$), $r_i = \sqrt{k_i/k_1}$ and $\eta_i = (b_e + b_{mi})/(2\sqrt{k_1 m})$ (see Table 15.1).

$$\begin{cases} r_1 = 1, \ \text{and} \ \ \eta_1 = 0.0074, & \text{for} \quad z < z_d \ (i = 1) \\ r_2 = \rho = \sqrt{20} \ \ \text{and} \ \ \eta_2 = 0.45, & \text{for} \quad z \geq z_d \ (i = 2) \end{cases} \tag{15.7}$$

The excitation frequency range used in simulation: $f_e = \frac{\omega_e}{2\pi} = (90-110)$Hz for crossing the resonant area, which was found at $f_e = f_n = \frac{\omega_1}{2\pi} = 94.8$Hz [13] ($f_n$ – natural frequency), (see Figs. 15.2).

The others parameters used in simulations are listed in table 15.1:

Table 15.1 System parameters

Symbol and value	Description
$m = 0.0038$kg	the effective mass of the magnet
$k_1 = 1348$N/m	the stiffness of the upper spring 1
$k_2 = 26960$N/m	the stiffness of the lower spring 2
$b_{m1} = 0.0175$Ns/m	the mechanical damping coefficient of the upper damper 1
$b_{m2} = 2.0208$Ns/m	the mechanical damping coefficient of the lower damper 2
$B = 0.57$T	the magnetic induction
$\ell = 0.44$m	the effective length of an electric coil
$R = 2.7\Omega$	the load resistance
$Rc = 1.2\Omega$	the internal resistance of an electric coil
$be = \frac{(B\ell)^2}{R+Rc}$	the electric damping coefficient
$\eta_i = \frac{b_e+b_{mi}}{2\sqrt{k_1 m}}$	the dimensionless damping coefficient of the system

15.3 The results of simulations

The essence of our non-linear systems is the appearance two solutions. In Fig. 15.2 a we show the resonance curve of the voltage output U versus excitation frequency. Note that the black one shows the results for the system without a stopper impacts at an enough large gap distance z_d. After shifting the gap to an appropriate smaller value, the stopper hits and the situation changes drastically. First of all the resonance region amplitude is limited to some value, but on the left hand side of the black curve we observe a substantial increase of the voltage output due to continuation of the impacting solutions (red curve) with increasing the excitation frequency. Simultaneously the second non-impacting solutions appear (blue curve and points) in the same region of frequency competing with the impacting one. This solution coincide with the black curve solution without a stopper. In Fig. 15.2b we show additionally a stroboscopic bifurcation diagram versus excitation frequency. It is possible to see that the impacting solution disappears entirely at the frequency f_e at about 106 Hz. Finally in Fig. 15.3a and b we show the corresponding time series and phase portraits for impacting and non-impacting solutions for chosen frequency at $f_e = 100$Hz, which depend on initial conditions. It confirms that for different initial conditions the mechanical resonator vibrates at different amplitudes and velocities respectively and so it leads to the larger or smaller voltage output. For distinguishing the different behaviour of the system in the case presented in Figs. 15.3, the dimensionless initial conditions $(\mathcal{Z}(\tau = 0), \dot{\mathcal{Z}}(\tau = 0)) = (z_0, \dot{z}_0)$ ware chosen in accordance to Fig. 15.4f as $z_0 = 0$, $\dot{z}_0 = 0$ (no impacts) and $z_0 = 1$, $\dot{z}_0 = 0$ (with impacts).

In the context of two competing solutions a new question arises. What are the basins of attraction of corresponding solutions and how they evolve with

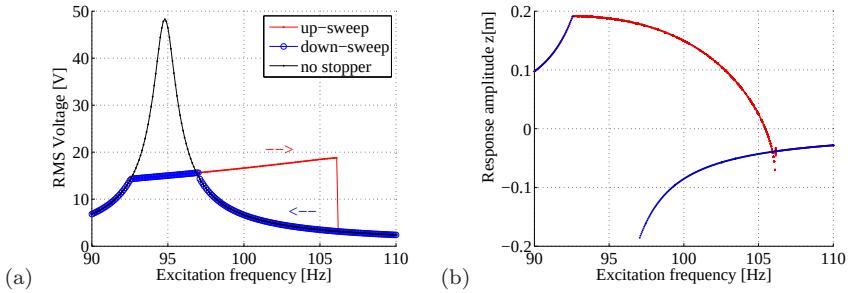

Fig. 15.2 RMS of voltage output versus frequency (a), blue colour denotes the solution with impacts for $f_e = (92.6 - 97.1)$Hz (swept by quasi-static decreasing of frequency) while red one corresponds to the impacting solution for $f_e = (92.6 - 106.1)$Hz (swept with increasing frequency), additionally black curve illustrates the solution without stopper. Bifurcation diagram (b).

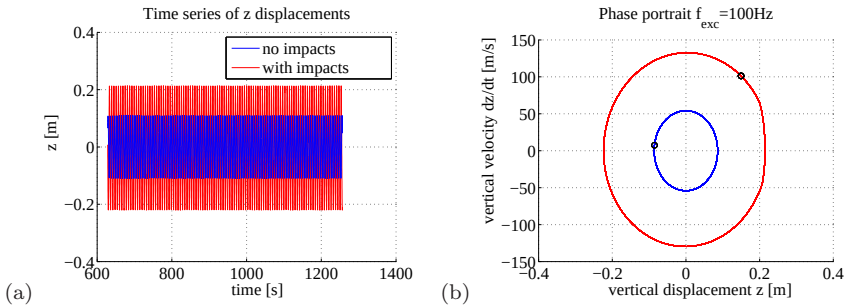

Fig. 15.3 Time series (a) and corresponding phase portraits with Poincare points (b) for two solutions. Blue colour denotes the solution without impacts while red one corresponds to the impacting solution.

increasing frequency. The answer to these questions clarifying the dynamics of two solutions is focussing the next part of our discussion.

For better clarity, the simulations were done for a number of initial conditions (Fig. 15.4) across the increasing frequency. Obviously the impacting solution basin (red colour) is fairly reduces by increasing excitation frequency and about $f_e = 106$ Hz it almost disappears. To follow the quantitative changes of basin size we defined by the size of the attractor as a corresponding fracture of an impacting solution basin to the whole rectangular surfaces (Fig. 15.4). These results are plotted in Fig. 15.5. Note, Figs. 15.4 and 15.5 show erosion in the basin of attraction with increasing frequency. One can clearly observe in Fig. 15.5, the erosion spreads increasingly out from the impacting solutions which are independent on initial conditions at f_e about 97 Hz (red background in Fig. 15.4a) to the solutions nearly without impacting (white background in Fig. 15.4i). This results provide detection of different behaviours due to double solutions phenomenon.

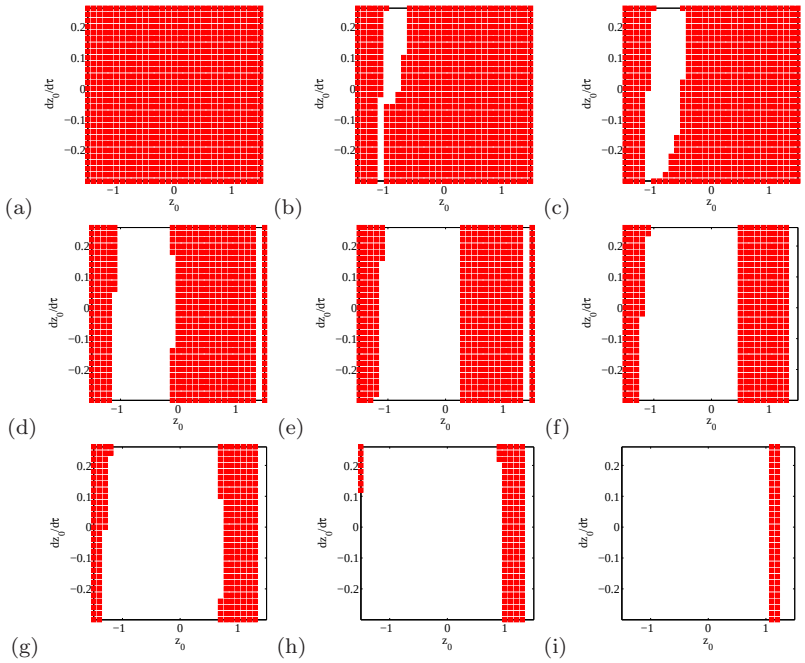

Fig. 15.4 Basins of attraction for impacting solution for increasing frequency: (a) $f_e = 97$ Hz, (b) $f_e = 97.2$ Hz, (c) $f_e = 97.4$ Hz, (d) $f_e = 98$ Hz, (e) $f_e = 99$ Hz, (f) $f_e = 100$ Hz, (g) $f_e = 102$ Hz, (h) $f_e = 105$ Hz, (i) $f_e = 106$ Hz. Note that in this figure, the dimensionless variables were used. Following Eq. 15.5 $(\mathcal{Z}(\tau = 0), \dot{\mathcal{Z}}(\tau = 0)) = (z_0, \dot{z}_0)$.

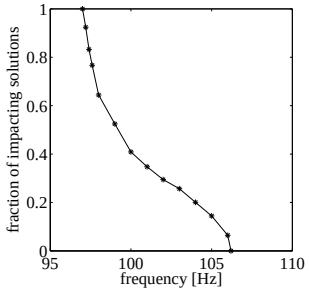

Fig. 15.5 Fraction of the impacting solution (basin of attraction) versus frequency.

15.4 Conclusions

In summary we note that the non-linear characteristics of the mechanical resonator with impacts provides a much broader frequency range for the power (RMS voltage in Fig. 15.2a). Two existing solutions (Fig. 15.2: with and without impacts) are characterized by different resonator amplitudes.

The results show that the basin of attraction for the impacting solution erodes strongly with the increasing frequency (Figs. 15.4 and 15.5). The influence of initial conditions on output energy is significant within the broaden band resonance curve, effecting multi-solution phenomenon.

A possible development of the proposed analysis consists in applying dynamical integrity arguments [14] to the basins of attraction reported in Fig. 15.4. This will allow us to detect the robustness of the two competing solutions with respect to changes in initial conditions, and thus will permit to judge on the reliability of the proposed system in harvesting energy.

Acknowledgement

The authors gratefully acknowledge the support of the 7th Framework Programme FP7-REGPOT-2009-1, under Grant Agreement No. 245479. MB and GL were partially supported by the Polish National Science Center under the grant No. 2012/05/B/ST8/00080.

References

1. S.P. Beeby, M.J. Tudor, N.M. White, *Measurement Science and Technology* 17 R175-R195 (2006).
2. P.D. Mitcheson, E.M. Yeatman, G.K. Rao, A.S. Holmes, T.C. Green, *Proc. IEEE* 96 1457-1486 (2008).
3. A. Erturk, D. Inman, Piezoelectric Energy Harvesting. Chichester: John Wiley & Sons Ltd. 2011.
4. S.P. Pellegrini, N. Tolu, M. Schenk, J.L. Herder, *J. Intellig. Mat. Syst. Struct.* doi: 10.1177/1045389X12444940 (2012).
5. B.P. Mann, D.A.W. Barton, B.A.M. Owens, *J. Intellig. Mat. Syst. Struct.* 23, 1451 (2012).
6. B.A.M. Owens, B.P. Mann, *J. Sound Vibr.* 331, 922 (2012).
7. D. Spreemann, Y. Manoli, Electromagnetic Vibration Energy Harvesting Devices, Springer, Berlin 2012.
8. L-C. J. Blystad, E Halvorsen, *Microsyst. Technol.* 17 505-511 (2011).
9. L. Gu, C Livermore, *J. Smart Mater. Struct.* 20, 045004 (2011).
10. C.P. Le, E. Halvorsen, O. Sorasen, E.M. Yeatman, *J. Intellig. Mat. Syst. Struct.* 23, 1409 (2012).
11. C.P. Le, E. Halvorsen, *J. Micromech. Microeng.* 22, 074006 12pp (2012).
12. M.S.M. Soliman, E.M. Abdel–Rahman, E.F. El–Saadany, R.R. Mansour, *J. Micromech. Microeng.* 18, 115021 11pp (2008).
13. M.S.M. Soliman, E.M. Abdel–Rahman, E.F. El–Saadany, R.R. Mansour, *J. Mirco-electromech. Systems* 18, 1288-1299 (2009).
14. S. Lenci, G. Rega, *Physica D* 240, 814–824 (2011).